

Assessing the Liquefaction Hazard in the Groningen Region of the Netherlands due to Induced Seismicity: Limitations of Existing Procedures and Development of a Groningen-Specific Framework

R.A. Green¹, J.J. Bommer², A. Rodriguez-Marek³, B.W. Maurer⁴,
P.J. Stafford⁵, B. Edwards⁶, P.P. Kruiver⁷, G. de Langes, and J. van Elk⁹

Abstract The Groningen gas field is one of the largest in the world and has produced over 2000 billion m³ of natural gas since the start of production in 1963. The first earthquakes linked to gas production in the Groningen field occurred in 1991, with the largest event to date being **M** 3.6. As a result, the field operator is leading an effort to quantify the seismic hazard and risk resulting from the gas production operations, including the assessment of liquefaction hazard. However, due to the unique characteristics of both the seismic hazard and the geological subsurface, particularly the unconsolidated sediments, direct application of existing liquefaction evaluation procedures is deemed inappropriate in Groningen. Specifically, the depth-stress reduction factor (r_d) and the Magnitude Scaling Factor (MSF) relationships inherent to existing variants of the simplified liquefaction evaluation procedure are considered unsuitable for use. Accordingly, efforts have first focused on developing a framework for evaluating the liquefaction potential of the region for magnitudes ranging from **M** 3.5 to 7.0. The limitations of existing liquefaction procedures for use in Groningen and the path being followed to overcome these shortcomings are presented in detail herein.

Keywords Liquefaction, liquefaction hazard, induced seismicity, Groningen gas field

¹Professor, Dept. of Civil and Environmental Engineering, Virginia Tech, Blacksburg, VA, USA (email: rugreen@vt.edu)

²Senior Research Investigator, Department of Civil and Environmental Engineering, Imperial College London, London, UK

³Professor, Dept. of Civil and Environmental Engineering, Virginia Tech, Blacksburg, VA, USA

⁴Assistant Professor, Dept. of Civil and Environmental Engineering, University of Washington, Seattle, WA, USA

⁵Reader, Dept. of Civil and Environmental Engineering, Imperial College London, London, UK

⁶Senior Lecturer, School of Environmental Sciences, University of Liverpool, Liverpool, UK

⁷Senior Geophysicist, Deltares, Delft, the Netherlands

⁸Senior Engineering Geologist, Deltares, Delft, the Netherlands

⁹Development Lead Groningen Asset, Nederlandse Aardolie Maatschappij B.V., Assen, the Netherlands

27 **1 Introduction**

28
29 The Groningen gas field is located in the northeastern region of the Netherlands and is one of the
30 largest in the world. It has produced over 2000 billion m³ of natural gas since the start of production
31 in 1963. The first earthquakes linked to gas production in the Groningen field occurred in 1991,
32 although earthquakes were linked to production at other gas fields in the region since 1986. To
33 date the largest induced earthquake due to production at the Groningen field is the 2012 moment
34 magnitude (**M**) 3.6 Huizinge event, and the largest recorded peak ground acceleration (PGA) is
35 0.11 g which was recorded during a more recent, smaller (local magnitude, **M_L**, 3.4) event. In
36 response to concerns about the induced earthquakes, the field operator Nederlandse Aardolie
37 Maatschappij (NAM) is leading an effort to quantify the seismic hazard and risk resulting from
38 the gas production operations (Bourne et al. 2015, van Elk et al. 2017). In view of the widespread
39 deposits of saturated sands in the region, the risk due to earthquake-induced liquefaction is being
40 evaluated as part of this effort. Although an almost negligible contributor to earthquake fatalities,
41 liquefaction triggering is an important threat to the built environment and in particular to
42 infrastructure and lifelines (e.g., Bird and Bommer 2004).

43
44 Central to the liquefaction hazard/risk assessment of the Groningen field is the stress-based
45 “simplified” liquefaction evaluation procedure, which is the most widely used approach to evaluate
46 liquefaction potential worldwide. While most of the recently proposed variants of this procedure
47 yield similar results for scenarios that are well represented in the liquefaction case history
48 databases (e.g., Green et al. 2014), their predictions deviate, sometimes significantly, for other
49 scenarios (e.g., low magnitude events; very shallow and very deep liquefiable layers; high fines
50 content soils; medium dense to dense soils). These deviations result partly because existing
51 variants of the simplified procedure are semi-empirical, hence they are apt for replicating existing
52 data but lack proper extrapolation power. The empirical elements of existing procedures are
53 derived from data from tectonic earthquakes in active shallow-crustal tectonic regimes such as
54 California, Japan, and New Zealand. These conditions are different from those that of the
55 Groningen field. Moreover, the geologic profiles/soil deposits in Groningen differ significantly
56 from those used to develop the empirical aspects of the simplified procedure. As a result, the
57 suitability of existing variants of the simplified procedure for direct use to evaluate liquefaction in

58 Groningen is questionable. Accordingly, prior to assessing the liquefaction hazard in Groningen,
59 efforts have first focused on developing a framework for performing the assessment. This actually
60 required a step backwards to develop an “unbiased” liquefaction triggering procedure for tectonic
61 earthquakes, due to biases in relationships inherent to existing variants of the simplified procedure
62 (e.g., Boulanger and Idriss 2014).

63
64 In the following sections, the shortcomings in current variants of the simplified procedures for use
65 in Groningen are detailed. Then, the efforts to develop a new “unbiased” variant of the simplified
66 liquefaction evaluation procedure are presented. An outline of how this procedure is being
67 modified for use in Groningen is presented next, followed by a brief overview of how the
68 liquefaction hazard of Groningen will be assessed.

69
70 **2 Shortcoming in existing variants of the simplified liquefaction evaluation procedure for**
71 **use in Groningen**

72
73 **2.1 Overview of the simplified procedure**

74
75 As mentioned in the Introduction, the stress-based simplified liquefaction evaluation procedure is
76 central to the approach adopted to assess the liquefaction hazard in the Groningen region. The
77 word “simplified” in the procedure’s title originated from the proposed use of a form of Newton’s
78 Second Law to compute cyclic shear stress (τ_c) imposed at a given depth in the soil profile, in lieu
79 of performing numerical site response analyses (Whitman 1971; Seed and Idriss 1971). Inherent
80 to this approach to computing the seismic demand is a depth-stress reduction factor (r_d) that
81 accounts for the non-rigid response of the soil profile and a Magnitude Scaling Factor (MSF) that
82 accounts for the effects of the shaking duration on liquefaction triggering. For historical reasons
83 the duration of an **M** 7.5 earthquake is used as the reference for MSF.

84
85 Case histories compiled from post-earthquake investigations were categorized as either
86 “liquefaction” or “no liquefaction” based on whether evidence of liquefaction was or was not
87 observed. The seismic demand (or normalized Cyclic Stress Ratio: CSR*) for each of the case
88 histories is plotted as a function of the corresponding normalized *in situ* test metric, e.g., Standard

89 Penetration Test (SPT): $N_{1,60cs}$; Cone Penetration Test (CPT): q_{c1Ncs} ; or small strain shear-wave
90 velocity (V_s): V_{s1} . In this plot, the “liquefaction” and “no liquefaction” cases tend to lie in two
91 different regions of the graph. The “boundary” separating these two sets of case histories is referred
92 to as the Cyclic Resistance Ratio ($CRR_{M7.5}$) and represents the capacity of the soil to resist
93 liquefaction during an **M** 7.5 event. This boundary can be expressed as a function of the normalized
94 *in situ* test metrics.

95
96 Consistent with the conventional definition for factor of safety (FS), the FS against liquefaction
97 (FS_{liq}) is defined as the capacity of the soil to resist liquefaction divided by the seismic demand:
98

$$FS_{liq} = \frac{CRR_{M7.5}}{CSR^*} \quad (1)$$

99
100 The Dutch National Annex to the Eurocode for the seismic actions (i.e., NPR 9998 2017),
101 recommends the use of the Idriss and Boulanger (2008) variant of the simplified liquefaction
102 evaluation procedure, but allows other variants to be used if they are in line with the safety
103 philosophy of the NPR 9998-2017. As a result, the Idriss and Boulanger (2008) variant and the
104 updated variant (Boulanger and Idriss 2014) have been used in several liquefaction studies in
105 Groningen, resulting in predictions of potentially catastrophic liquefaction effects that have severe
106 implications for buildings and for infrastructure such as dikes.

107

108 **2.2 Depth-stress reduction factor: r_d**

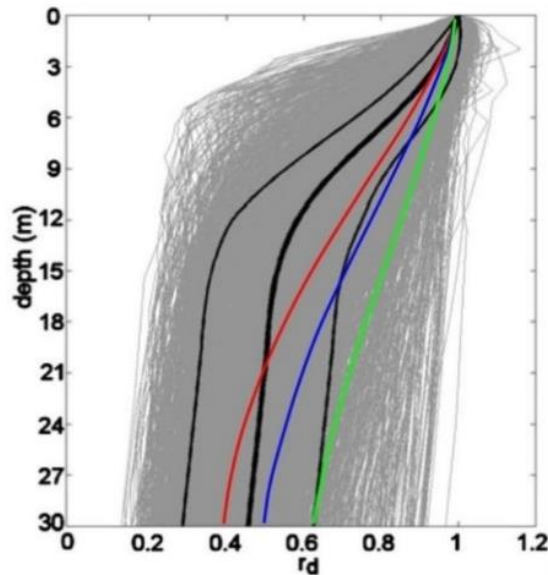
109

110 As stated above, r_d is an empirical factor that accounts for the non-rigid response of the soil profile.
111 Both the Idriss and Boulanger (2008) and Boulanger and Idriss (2014) variants of the simplified
112 liquefaction evaluation procedure use an r_d relationship that was developed by Idriss (1999). As
113 shown in Figure 1, the Idriss (1999) r_d relationship is a function of earthquake magnitude and
114 depth, with r_d being closer to one for larger magnitude events (note that $r_d = 1$ for all depths
115 corresponds to the rigid response of the profile). This is because larger magnitude events have
116 longer characteristic periods and, hence, ground motions with longer wave lengths. As a result,
117 even a soft profile will tend to respond as a rigid body if the characteristic wave length of the
118 ground motions is significantly longer than the overall thickness of the profile. Accordingly, the

119 correlation between earthquake magnitude and the frequency content of the earthquake motions
120 significantly influences the r_d relationship. This raises questions regarding the appropriateness of
121 the Idriss (1999) relationship, which was developed using motions recorded during tectonic events,
122 for evaluating liquefaction potential in Groningen where the seismic hazard is dominated by
123 induced earthquakes having magnitudes less than M 5.

124
125 Another issue with the Idriss (1999) r_d relationship is that it tends to predict overly high CSR^*
126 values at depth in a soil profile for tectonic events. This bias is illustrated in Figure 1 and is
127 pronounced for depths between ~ 3 to 20 m below the ground surface. As a result, when used to
128 evaluate case histories to develop the $CRR_{M7.5}$ curves that are central to the procedure, the biased
129 r_d relationship results in a biased positioning of the $CRR_{M7.5}$ curve. The significance of this issue
130 is mitigated to some extent when the same r_d relationship used to develop the $CRR_{M7.5}$ curve is
131 also used in forward analyses (i.e., the bias cancels out). However, this will not be the case if
132 site/region-specific r_d relationships are developed and used in conjunction with a $CRR_{M7.5}$ curve
133 that was developed using a “biased” r_d relationship.

134



135
136 **Fig. 1** The red, blue, and green lines were computed using the Idriss (1999) r_d relationship for M
137 5.5, M 6.5, and M 7.5 events, respectively. The grey lines were computed by Cetin (2000) from
138 equivalent linear site response analyses performed using a matrix of 50 soil profiles and 40
139 motions. The black lines are the median (thick line) and median plus/minus one standard deviation

140 (thinner lines) for the Cetin (2000) analyses.

141

142 **2.3 Magnitude Scaling Factor: MSF**

143

144 As stated above, MSFs account for the influence of the strong motion duration on liquefaction
145 triggering. MSFs have traditionally been computed as the ratio of the number of equivalent cycles

146 for an **M** 7.5 event to that of a magnitude **M** event, raised to the power *b* [i.e., $MSF=(n_{eqM7.5}/n_{eqM})^b$].

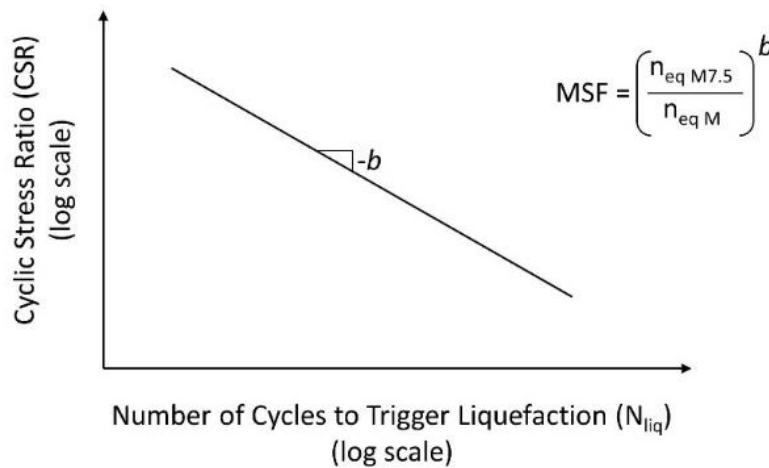
147 Both the Idriss and Boulanger (2008) and Boulanger and Idriss (2014) procedures used the Seed
148 et al. (1975) variant of the Palmgren-Miner (P-M) fatigue theory to compute $n_{eqM7.5}$ and n_{eqM} from

149 earthquake motions recorded at the surface of soil profiles. Furthermore, they obtained the value
150 of *b* from laboratory test data. The parameter *b* is the negative of the slope of a plot of log(CSR)

151 versus log(N_{liq}), as shown in Figure 2; N_{liq} is the number of cycles required to trigger liquefaction
152 in a soil specimen subjected to sinusoidal loading having an amplitude of CSR, typically

153 determined using cyclic triaxial or cyclic simple shear tests.

154



155

156 **Fig. 2** Relationship between laboratory CSR vs. N_{liq} and MSF.

157

158 There are several shortcomings inherent to the approach used by Idriss and Boulanger (2008) and
159 Boulanger and Idriss (2014) to compute the number of equivalent cycles and MSF. These include:

- 160 • Both the magnitude and uncertainty of n_{eq} , and hence MSF, are assumed to be constant with
161 depth. However, Green and Terri (2005) have shown that n_{eq} can vary with depth in a given
162 profile and Lasley et al. (2017) showed that while the median value for n_{eq} computed for a

163 large number of soil profiles and ground motions is relatively constant with depth, the
164 uncertainty in n_{eq} varies with depth.

- 165 • Pulses in the acceleration time history having an amplitude less than $0.3 \cdot a_{max}$ are assumed not
166 to contribute to the triggering of liquefaction, and thus are not considered in the computation
167 of n_{eq} . Using a relative amplitude criterion to exclude pulses is contrary to the known nonlinear
168 response of soil which is governed by the absolute amplitude of the imposed load, among other
169 factors. The use of a relative amplitude exclusion criterion with tectonic earthquake motions
170 may inherently bias the resulting MSF.
- 171 • Each of the two horizontal components of ground motion is treated separately, inherently
172 assuming that both components have similar characteristics. However, analysis of recorded
173 motions has shown this is not always the case, particularly in the near fault region (e.g., Green
174 et al. 2008; Carter et al. 2016). Groningen ground-motions recorded at short source-to-site
175 distances often display pronounced polarization (Stafford et al. 2018).
- 176 • The b values used by Boulanger and Idriss (2014) were derived from several laboratory studies
177 performed on various soils and it is uncertain whether all these studies used a consistent
178 definition of liquefaction in interpreting the test data. As a result, the b values proposed by
179 Boulanger and Idriss (2014) entail considerable uncertainty (Ulmer et al. 2018), with the
180 proposed values not being in accord with those inherent to the shear modulus and damping
181 degradation curves used in the equivalent linear site response analyses to develop the r_a
182 correlations (a point elaborated upon subsequently).
- 183 • Recent studies have shown that the residuals of the amplitude and duration of earthquake
184 ground motions are negatively correlated (e.g., Bradley 2011) and this feature is clearly
185 observed in the Groningen data (Bommer et al. 2016). None of the MSF correlations developed
186 to date, to include the one proposed by Boulanger and Idriss (2014), have considered this.

187
188 Some of the shortcomings listed above will be more significant to the Groningen liquefaction
189 hazard assessment than others, but it is difficult to state *a priori* which ones these are. Furthermore,
190 even for tectonic earthquakes the validation of MSF relationships is hindered by the limited
191 magnitude range of case histories in the field liquefaction databases, with the majority of the cases
192 being for events having magnitudes ranging from **M** 6.25 to **M** 7.75 (NRC 2016). Specific to the
193 Groningen liquefaction hazard assessment, MSFs for small magnitude events are very important,

194 particularly given that published MSF relationships vary by a factor of 3 for M 5.5 (Youd et al.
195 2001), with this factor increasing if the proposed MSF relations are extrapolated to lower
196 magnitudes.

197

198 **3 Removing bias from the simplified liquefaction evaluation procedure for tectonic** 199 **earthquakes**

200

201 **3.1 Depth-stress reduction factor: r_d**

202

203 A new relationship for r_d was developed by Lasley et al. (2016) using an approach similar to that
204 used by Cetin (2000). Equivalent linear site response analyses were performed on 50 soil profiles
205 compiled by Cetin (2000) that are representative of those in the liquefaction case history databases.
206 However, Lasley et al. (2016) used a larger set of recorded input motions in their analyses than
207 were available at the time of the Cetin (2000) study. Several functional forms for r_d were examined
208 by Lasley et al. (2016) in regressing the results from the site response analyses, with the following
209 form selected because of its simplicity and fit of the data (i.e., relatively low standard deviation of
210 the regressed data):

211

$$r_d = (1 - \alpha) \exp\left(\frac{-z}{\beta}\right) + \alpha + \varepsilon_{r_d} \quad (2a)$$

212

213 where z is depth in meters, α is the limiting value of r_d at large depths and can range from 0 to 1,
214 the variable β controls the curvature of the function at shallow depths, and ε_{r_d} is a zero-mean
215 random variable with standard deviation σ_{r_d} . Expressions for α and β are:

216

$$\alpha = \exp(-4.373 + 0.4491 \cdot M) \quad (2b)$$

$$\beta = -20.11 + 6.247 \cdot M \quad (2c)$$

217

218 and σ_{r_d} is defined as:

219

$$\sigma_{r_d} = \frac{0.1506}{[1 + \exp(-0.4975 \cdot z)]} \quad (2d)$$

220
221 Relative to the other r_d relationships inherent to commonly used variants of the simplified
222 procedure, the Lasley et al. (2016) model was developed using more site response data and more
223 rigorous regression analyses. So while all relationships inherently have some bias, a strong
224 argument can be made that Lasley et al. (2016) has the least bias of commonly used relationships
225 and was therefore adopted for use herein.

226

227 **3.2 Magnitude Scaling Factor: MSF**

228

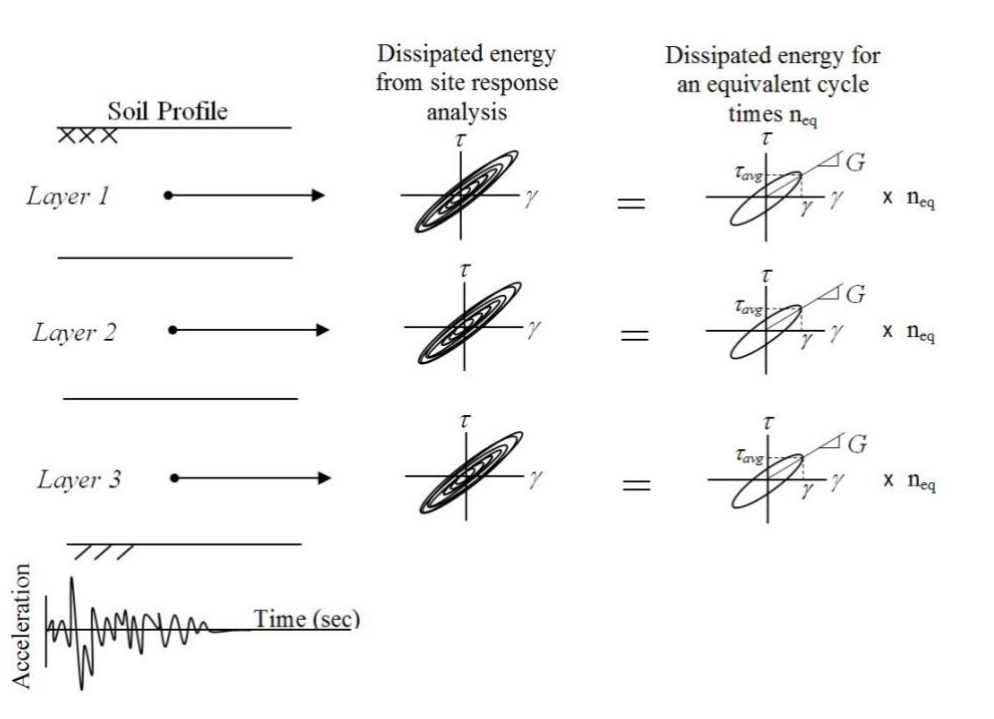
229 Development of a MSF relationship that overcomes all the shortcomings listed above for the Idriss
230 and Boulanger (2008) and Boulanger and Idriss (2014) relationships is not as straightforward as
231 developing the new r_d relationships. The reason for this is that there are many more issues with
232 existing MSFs than there are with the r_d relationships. As a result, a new approach needed to be
233 used to compute MSFs, as opposed to implementing an existing approach using a more
234 comprehensive dataset and a more rigorous regression analysis.

235

236 As mentioned previously and shown in Figure 2, MSFs are computed from equivalent number of
237 cycles, n_{eq} . Well-established fatigue theories have been proposed for computing n_{eq} for materials
238 having varying phenomenological behaviour; reviews of different approaches for computing n_{eq}
239 are provided in Green and Terri (2005) and Hancock and Bommer (2005), among others.
240 Developed specifically for use in evaluating liquefaction potential, the approach proposed by
241 Green and Terri (2005) was selected for developing an n_{eq} relationship for the Groningen project.
242 This approach is an alternative implementation of the P-M fatigue theory that better accounts for
243 the nonlinear behaviour of the soil than the Seed et al. (1975) variant. In this approach, dissipated
244 energy is explicitly used as the damage metric. n_{eq} is determined by equating the energy dissipated
245 in a soil element subjected to an earthquake motion to the energy dissipated in the same soil
246 element subjected to a sinusoidal motion of a given amplitude and a “duration” of n_{eq} . Dissipated
247 energy was selected as the damage metric because it has been shown to correlate with excess pore
248 pressure generation in saturated cohesionless soil samples subjected to undrained cyclic loading
249 (e.g., Green et al. 2000; Polito et al. 2008). Furthermore, from a microscopic perspective, the
250 energy is thought to be predominantly dissipated by the friction between sand grains as they move

251 relative to each other as the soil skeleton breaks down, which is requisite for liquefaction
 252 triggering.

253
 254 Conceptually, the Green and Terri (2005) approach for computing n_{eq} is shown in Figure 3. Stress
 255 and strain time-histories at various depths in the soil profile are obtained from a site response
 256 analysis. By integrating the variation of shear stress over shear strain, the cumulative dissipated
 257 energy per unit volume of soil can be computed (i.e., the cumulative area bounded by the shear
 258 stress-shear strain hysteresis loops). n_{eq} is then determined by dividing the cumulative dissipated
 259 energy for the entire earthquake motion by the energy dissipated in one equivalent cycle. For
 260 historical reasons, the shear stress amplitude of the equivalent cycle (τ_{avg}) is taken as $0.65 \cdot \tau_{max}$
 261 (where τ_{max} is the maximum induced cyclic shear stress, τ_c , at a given depth), and the dissipated
 262 energy associated with the equivalent cycle is determined from the constitutive model used in the
 263 site response analysis.



264
 265 **Fig. 3** Illustration of the proposed procedure to compute n_{eq} . In this procedure, the energy
 266 dissipated in a layer of soil, as computed from a site response analysis, is equated to the energy
 267 dissipated in an equivalent cycle of loading multiplied by n_{eq} .

268
 269 As noted above, one of the shortcomings of the Seed et al. (1975) variant of the P-M fatigue theory

270 is the way in which multi-directional shaking is taken into account. Specifically, each of the two
 271 horizontal components of ground motion is treated separately, inherently assuming that both
 272 components have similar characteristics. However, analysis of recorded motions has shown this is
 273 not always the case, particularly in the near fault region (e.g., Green et al. 2008; Carter et al. 2016).
 274 In contrast, Green and Terri (2005) accounted for multi-directional shaking by performing separate
 275 site response analyses for each horizontal component in a pair of motions, adding the energy
 276 dissipated at the respective depths for each component of motion, and setting the amplitude of the
 277 equivalent cycle as 0.65 times the geometric mean of the maximum shear stresses experienced at
 278 a given depth. This approach is referred to as “Approach 2” in Lasley et al. (2017) and is used
 279 herein because it better accounts for differences in the characteristics in the two horizontal
 280 components of motion.

281
 282 Lasley et al. (2017) implemented the Green and Terri (2005) approach for computing n_{eq} using the
 283 same motions and profiles used by Lasley et al. (2016) to develop their r_d relationship. Their
 284 proposed n_{eq} relationship is:

$$\ln(n_{eq}) = 0.4605 - 0.4082 \cdot \ln\left(\frac{a_{max}}{g}\right) + 0.2332 \cdot M + \varepsilon_{Total} \quad (3a)$$

286
 287 where a_{max} is in units of g and ε_{Total} is a zero-mean random variable with standard deviation σ_{Total}
 288 given by:

$$\sigma_{Total}(z) = \max\left[0.5399 - \frac{z}{26.4} (0.5399 - 0.4626), 0.4626\right] \quad (3b)$$

290
 291
 292 where z is depth in meters. The dependency of n_{eq} on a_{max} in Eq. 3 was chosen because of the
 293 observed negative correlation of strong ground-motion duration with a_{max} (e.g., Bradley 2011).
 294 Also, the functional form of this correlation is not an impediment to implementation because the
 295 simplified liquefaction evaluation procedures require both the magnitude (for MSFs and r_d) and
 296 a_{max} as input variables.

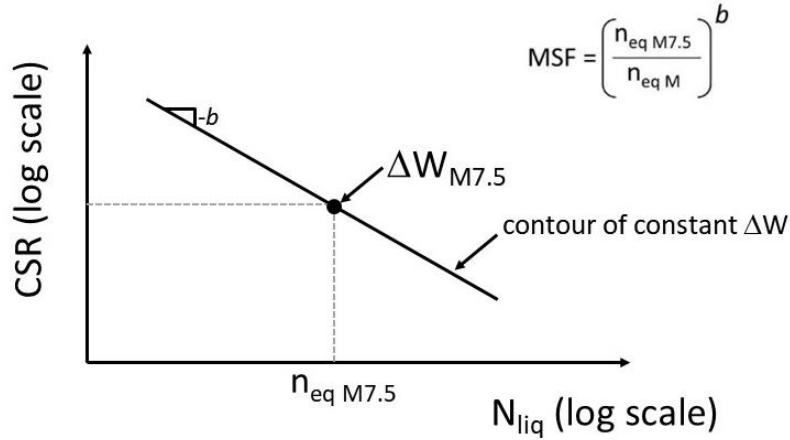
297
298
299
300
301
302

303
304
305
306
307
308
309
310
311
312
313
314
315
316
317
318
319
320
321
322
323
324

The b value that is needed to relate n_{eq} to MSFs (e.g., Figure 2) can also be determined from the constitutive model used in the site response analysis, by assuming that the CSR vs. N_{liq} curve shown in Figure 2 is a contour of constant dissipated energy (Figure 4). In Figure 4, the dissipated energy for a **M** 7.5 earthquake, $\Delta W_{M7.5}$, is computed using:

$$\Delta W_{M7.5} = \frac{2\pi \cdot D_\gamma \cdot \tau_c^2}{G_{max} \cdot \left(\frac{G}{G_{max}}\right)_\gamma} \cdot n_{eq\ M7.5} \tag{4}$$

where D_γ is the damping ratio for the induced shear strain γ , τ_c is the cyclic shear stress and G is the secant shear modulus. This equation is based on the assumption that the soil can be modelled as a visco-elastic material, consistent with the assumption inherent to the equivalent linear site response algorithm. For liquefaction evaluations, τ_c used to compute $\Delta W_{M7.5}$ can be determined from the $CRR_{M7.5}$ curve from the simplified liquefaction evaluation procedure (e.g., Boulanger and Idriss 2014). Accordingly, the computed CSR vs. N_{liq} curve corresponds to a soil having a given q_{c1Ncs} and confined at an initial effective overburden stress (σ'_{vo}) (i.e., $\tau_c = CRR_{M7.5} \times \sigma'_{vo}$); the small strain shear modulus (G_{max}) for the soil should be consistent with the penetration resistance used to determine $CRR_{M7.5}$. The damping (D_γ) and the degraded secant shear modulus, $G_{max} \cdot (G/G_{max})_\gamma$, values in Eq. (4) are commensurate with the induced shear strain (γ) in the soil and can be determined iteratively from the shear modulus and damping degradation curves used to model the soil response (e.g., Darendeli and Stokoe 2001). Once the value of $\Delta W_{M7.5}$ is determined, a contour of constant dissipated energy can be computed for different amplitudes of loading by simply computing the number of cycles for the assumed loading amplitude required for the dissipated energy to equal $\Delta W_{M7.5}$. The parameter b is assumed equal to the negative of the slope of the contour of constant dissipated energy. The assumption that the CSR vs. N_{liq} curve is a contour of constant dissipated energy inherently implies that the energy dissipated in a given element of soil at the point of liquefaction triggering is unique and independent of the imposed loading characteristics. Several studies have shown that this is a reasonable assumption (e.g., Kokusho and Kaneko 2014; Polito et al. 2013).



325
 326 **Fig. 4** A CSR vs. N_{liq} curve can be computed from shear modulus and damping degradation curves
 327 assuming the curve is a contour of constant dissipated energy. $\Delta W_{M7.5}$ can be computed using Eq.
 328 (4) and the remaining portions of the curve can be computed for different amplitudes of loading
 329 by simply computing the number of cycles for the assumed loading amplitude required for the
 330 dissipated energy to equal $\Delta W_{M7.5}$.

331
 332 The degradation curves proposed Darendeli and Stokoe (2001) were used herein to determine the
 333 b values following the procedure illustrated in Figure 4 for a range of effective confining stresses
 334 and soil densities, with the resulting values ranging from 0.33 to 0.35. However, $b = 0.34$ for the
 335 vast majority of the confining stress-density combinations considered and was thus used herein to
 336 compute MSFs from n_{eq} . Additionally, $b = 0.34$ is consistent with laboratory curves developed
 337 from high-quality undisturbed samples obtained by freezing (Yoshimi et al. 1984). Accordingly,
 338 MSFs herein are computed as:

339

$$MSF = \left(\frac{n_{eq M7.5}}{n_{eq M}} \right)^b = \left(\frac{14}{n_{eq M}} \right)^{0.34} \leq 2.02 \quad (5a)$$

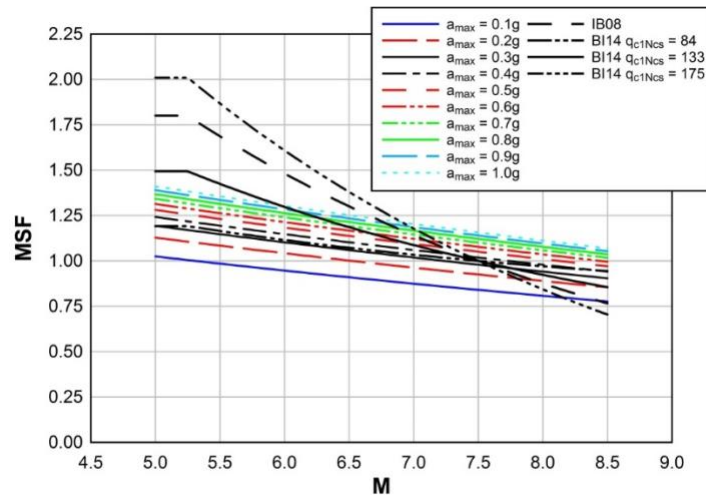
$$\sigma_{\ln(MSF)} = b \cdot \sigma_{\ln(n_{eq M})} = 0.34 \cdot \sigma_{\ln(n_{eq M})} \quad (5b)$$

340
 341 where $\sigma_{\ln(MSF)}$ is a first order approximation for the standard deviation of the natural log of the
 342 MSF, and $n_{eq M}$ and $n_{eq M7.5}$ are computed using Eq. (3).

343
 344 To compute $n_{eq M7.5}$ using Eq. (3), M is set to 7.5 and a corresponding value for a_{max} needs to be

345 assumed (i.e., $a_{max7.5}$). The value of $a_{max7.5}$ was determined by computing the average a_{max} for the
 346 case histories in the Boulanger and Idriss (2014) SPT and CPT liquefaction case history databases
 347 ranging in magnitude from M 7.4 to 7.6. The average a_{max} for the 116 case histories that fell within
 348 this magnitude range was ~ 0.35 g. Using this value for $a_{max7.5}$, $n_{eq M7.5}$ was computed to be ~ 14 .
 349 This value is similar to that determined by Seed et al. (1975), i.e., $n_{eq M7.5} = 15$. However, the value
 350 reported by Seed et al. (1975) represents the average for two horizontal components of motion,
 351 while the value computed herein represents the combined influence of both components of motion
 352 (Approach 2, Lasley et al. 2017). As a result, the value computed herein is approximately half of
 353 that computed by Seed et al. (1975). This difference is due both to the significantly larger ground
 354 motion database used by Lasley et al. (2017) to develop Eq. (3), where the motions used by Lasley
 355 et al. (2017) represented a broader range of magnitudes and site-to-source distances compared to
 356 those used by Seed et al. (1975), and to the differences in the approaches used to compute n_{eq} .
 357 However, both of these differences also influence the denominator in Eq. (5a), which minimizes
 358 their influence on the resulting MSF. The upper limit on the MSF (i.e., 2.02) corresponds to a
 359 scenario where the earthquake motions consist of a single shear stress pulse in one of the horizontal
 360 components of motion. A plot of Eq. (5a) is shown in Figure 5 for magnitudes ranging from M 5.0
 361 to 8.5 and a_{max} ranging from 0.1 to 1.0 g.

362



363

364 **Fig. 5** For a given magnitude earthquake, MSF developed herein increases as a_{max} increases. Also,
 365 for comparison, the MSFs proposed by Idriss and Boulanger (2008) (IB08) and Boulanger and
 366 Idriss (2014) (BI14) are also shown.

367

368 Figure 5 also shows a comparison of the MSF developed herein with those proposed by Idriss and
 369 Boulanger (2008) and Boulanger and Idriss (2014), where the latter is shown for $q_{c1Ncs} = 84, 133,$
 370 and 175 atm. As may be observed from this figure, for a given value of a_{max} the MSF developed
 371 herein has about the same dependency on magnitude as the MSF proposed by Boulanger and Idriss
 372 (2014) for $q_{c1Ncs} = 84$ atm (i.e., medium dense sand). However, the difference between the two is
 373 that the former is a function of a_{max} , with MSF for a given magnitude increasing as a_{max} increases.

374

375 **3.3 “Unbiased” $CRR_{M7.5}$ curve**

376

377 The Lasley et al. (2016) r_a relationship and the MSF relationship developed herein were used to
 378 reanalyse the CPT liquefaction case history database compiled by Boulanger and Idriss (2014); all
 379 other parameters/relationships used to analyse the case history data were the same as those used
 380 by Boulanger and Idriss (2014). These case histories were then used to regress a new “unbiased”
 381 deterministic liquefaction triggering curve (i.e., $CRR_{M7.5}$ curve), which is shown in Figure 6. This
 382 curve approximately corresponds to a probability of liquefaction [P(liq)] of 35% (total uncertainty)
 383 and is given by:

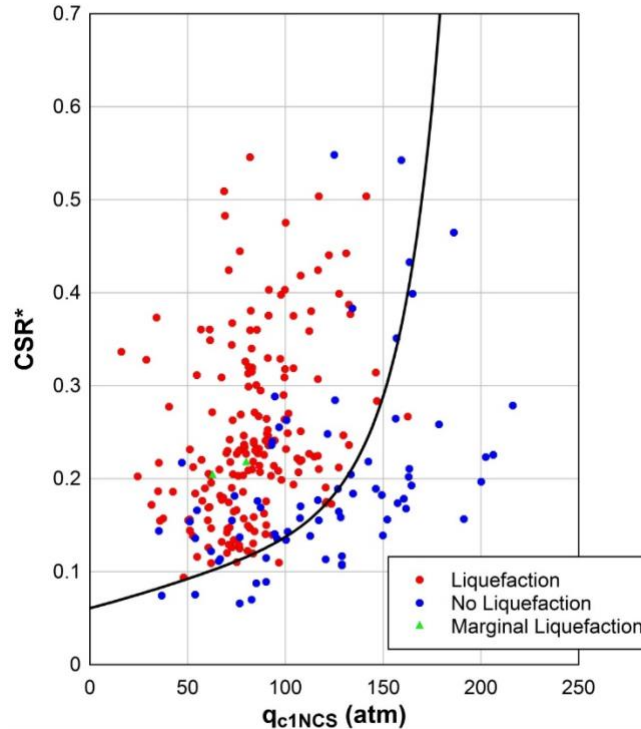
384

$$CRR_{M7.5} = \exp \left\{ \left(\frac{q_{c1Ncs}}{113} \right) + \left(\frac{q_{c1Ncs}}{1000} \right)^2 - \left(\frac{q_{c1Ncs}}{140} \right)^3 + \left(\frac{q_{c1Ncs}}{137} \right)^4 - 2.8118706 \right\} \leq 0.6 \quad (6)$$

385

386 where q_{c1Ncs} is computed using the procedure outlined in Boulanger and Idriss (2014).

387



388

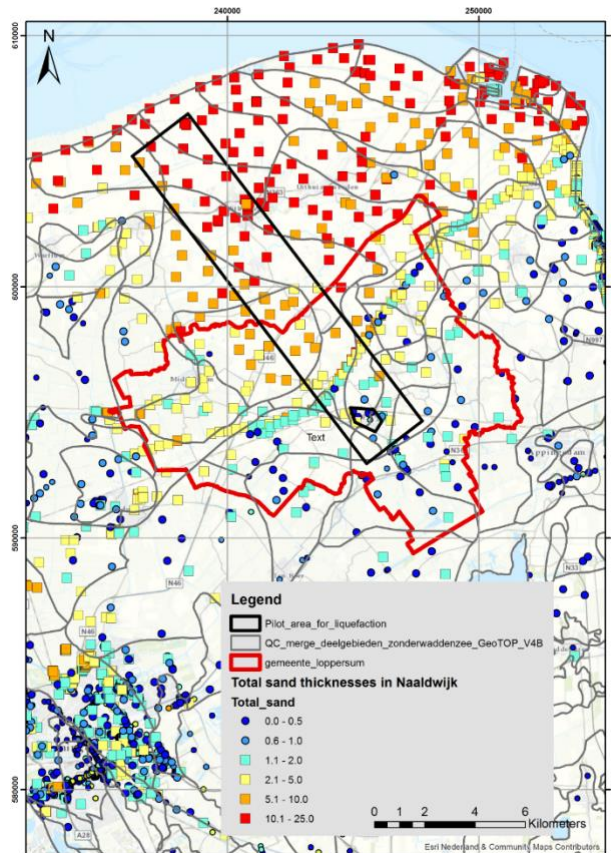
389 **Fig. 6** “Unbiased” deterministic $CRR_{M7.5}$ curve regressed from liquefaction case history data from
 390 Boulanger and Idriss (2014) that were reanalysed using Lasley et al. (2016) r_d relationship and
 391 MSF developed herein.

392

393 **4 Assessment of liquefaction hazard in Groningen**

394

395 To determine whether a Groningen-wide liquefaction hazard assessment is warranted, a
 396 liquefaction hazard pilot study is being performed first, wherein the study area was selected to
 397 simultaneously satisfy three criteria: (a) proximity to the region of highest shaking hazard; (b)
 398 sampling of areas with sand deposits that are thick, shallow, young, and loose; and (c) sampling
 399 of multiple site-response zones used in developing the Groningen-specific ground-motion model
 400 (Rodriguez-Marek et al. 2017). The location of the pilot study area is shown in Figure 7, along
 401 with the cumulative thicknesses of the Holocene sand deposits that comprise the Naaldwijk
 402 formation which is considered to have the highest liquefaction potential in the region (Korff et al.
 403 2017). However, before the liquefaction pilot study can be performed, Groningen-specific r_d and
 404 MSF relationships must be developed following the approaches used by Lasley et al. (2016, 2017)
 405 and presented above. The soil/geologic profiles and ground motions used to develop the
 406 Groningen-specific relationships are detailed below.



408

409 **Fig. 7** Location of the liquefaction pilot study area across the Groningen gas field. Also shown are
 410 the cumulative thicknesses of the Holocene sand deposits that comprise the Naaldwijk formation.

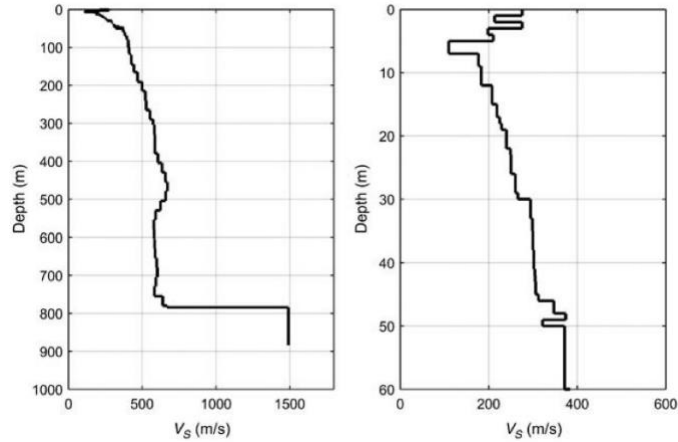
411

412 **4.1 Groningen-specific r_a and MSF relationships**

413

414 The geological setting of Groningen, including detailed cross sections, is described in Kruiver et
 415 al. (2017a), and the velocity model from the selected reference rock horizon (at ~ 800 m depth) to
 416 the ground surface is described in detail by Kruiver et al. (2017b). An example of the resulting V_s
 417 profiles is shown in Figure 8. The unit weights of the strata in the profiles are also needed for the
 418 site response analyses. Towards this end, the assignment of unit weight is based on representative
 419 values for stratigraphic lithological units derived from CPTs using Lunne et al. (1997). For some
 420 of the deeper formations, the density is assumed to be constant, consistent with the borehole logs
 421 from two deep boreholes (Kruiver et al., 2017a, b).

422



423
 424 **Fig. 8** Sample Vs profile at the location of one of the many ground-motion recording stations in
 425 the field. The plot on the left is the full profile down to reference rock horizon (depth of ~800 m),
 426 and the plot on the right is an enlarged view of the upper 60 m of the profile. (Rodriguez-Marek et
 427 al. 2017)

428
 429 The software SMSIM (Boore 2005, version 16/12/2009) was used in conjunction with the
 430 Groningen-specific model parameters to generate motions at the reference horizon (Bommer et al.
 431 2017) for magnitudes ranging from **M** 3.5 to 7.0 and epicentral distances ranging from 0.1 to 60
 432 km. The lower bound was chosen on the basis of no liquefaction having been observed in the field
 433 to date and to explore the full range of potential triggering events, despite the fact that globally
 434 there is no reliable evidence of liquefaction triggering by earthquakes smaller than **M** 4.5 (Green
 435 and Bommer 2018). The upper value in the maximum magnitude distribution is **M** 7.25 as
 436 determined by an expert panel (Bommer and van Elk 2017).

437
 438 Once developed, the Groningen-specific r_d and MSF relationships can be used in conjunction with
 439 the $CRR_{M7.5}$ curve shown in Figure 6 to compute the FS_{liq} at depth in profiles in Groningen
 440 subjected to induced earthquake motions. The computation of liquefaction hazard curves that will
 441 be used to determine whether the hazard due to liquefaction is significant enough to require the
 442 consequences from liquefaction to be assessed is discussed next.

443
 444
 445
 446

4.2 Planned output from the liquefaction hazard study

The liquefaction hazard will be calculated using a Monte Carlo method (Bourne et al. 2015) wherein probability distributions for activity rates (Bourne and Oates 2017), event locations and magnitudes, and resulting ground motions will be sampled such that the simulated future seismic hazard is consistent with historical seismic and reservoir compaction datasets. For each event scenario, the developed Groningen-specific relationships will be used to compute the FS_{liq} as a function of depth for ~100 profiles across the pilot study area.

The “Ishihara inspired LPI” (LPI_{ish}) framework will be used to relate computed FS_{liq} to the predicted the severity of surficial liquefaction manifestation, which has been shown to correlate to liquefaction damage potential for level ground sites. The LPI_{ish} framework was proposed by (Maurer et al. 2015a) and is a conceptual and mathematical merger of the Ishihara (1985) H_1 - H_2 chart and Liquefaction Potential Index (LPI) framework (Iwasaki et al. 1978). The most notable differences between the original LPI and LPI_{ish} frameworks are that the latter better accounts for the influence of the non-liquefiable crust on the severity of surficial liquefaction manifestations (Green et al. 2018) and more appropriately weights the contribution of shallower liquefied layers to surficial manifestations (van Ballegooy et al. 2014). The LPI_{ish} framework was chosen for this study because it has been shown to yield more accurate predictions of the severity of surficial liquefaction manifestations than competing indices (Maurer et al. 2015a, b): LPI (Iwasaki et al. 1978) and LSN (van Ballegooy et al. 2014).

The output from the liquefaction pilot study will be liquefaction hazard curves for the ~100 sites in the study area, where the hazard curves show the annual frequency of exceedance (AFE) of varying LPI_{ish} values for a site. Consistent with the requirements of NPR 9998-2017 (NPR 9998 2017), which was specifically for the Groningen field, LPI_{ish} values corresponding to an AFE of $\sim 4 \times 10^{-4}$ (or a 2475-year return period) will be of interest. The results from this pilot study will differ from previous liquefaction studies performed for Groningen, where liquefaction was evaluated in previous studies for earthquake scenarios (i.e., ground motions and magnitudes) corresponding to a given return period (i.e., a “pseudo-probabilistic” approach).

478 The optimal LPI_{ish} thresholds corresponding to different severities of surficial liquefaction
479 manifestations are dependent on the liquefaction triggering procedure used to compute FS_{liq} and
480 the characteristics of the profile. However, without liquefaction case history data to develop
481 Groningen-specific thresholds, the thresholds proposed by Iwasaki et al. (1978) will be
482 conservatively (Maurer et al. 2015c) used in the pilot study with the LPI_{ish} framework (i.e., LPI_{ish}
483 < 5 : none to minor surficial liquefaction manifestations are predicted; $LPI_{ish} > 15$: severe surficial
484 liquefaction manifestations are predicted).

485

486 **5 Discussion and conclusions**

487

488 The presence of saturated loose deposits of young sands in the Groningen field region creates the
489 necessity to assess the potential for liquefaction triggering by the earthquakes being induced by
490 the gas production as an integral component of the seismic risk analysis. The application of
491 liquefaction hazard assessment procedures calibrated for larger-magnitude tectonic earthquakes in
492 other regions has resulted in predictions of potentially catastrophic liquefaction effects, with severe
493 implications for buildings and for infrastructure such as dikes. Despite the fact these estimates,
494 sometimes associated with earthquake scenarios only fractionally greater than the lower bound for
495 events that have been observed globally to trigger liquefaction that poses a threat to the built
496 environment (Green and Bommer 2018), the dissemination of such results has raised great concern
497 regarding liquefaction hazard in Groningen.

498

499 Due to the unique characteristics of both the seismic hazard and the geologic profiles/soil deposits
500 in Groningen, direct application of existing variants of the simplified liquefaction evaluation
501 procedure is deemed inappropriate for assessing the liquefaction hazard of the region, including
502 the Idriss and Boulanger (2008) procedure recommended in the NPR 9998-2017 and the updated
503 variant, Boulanger and Idriss (2014). Accordingly, efforts were first focused on re-analyzing the
504 liquefaction case histories that were compiled for natural earthquakes to remove bias in their
505 interpretation. Towards this end, new a depth-stress reduction factor (r_d) and number of equivalent
506 cycles (n_{eq})/magnitude scaling factor (MSF) relationships for shallow crustal active tectonic
507 regimes were developed and used in the reanalysis of the cone penetration test (CPT)
508 “liquefaction” and “no liquefaction” case histories compiled by Boulanger and Idriss (2014). These

509 case histories were then used to regress a new “unbiased” deterministic liquefaction triggering
510 curve (or cyclic resistance ratio curve: $CRR_{M7.5}$). The “unbiased” procedure can be readily adapted
511 to evaluate liquefaction potential in regions with unique profiles and/or ground motions, such as
512 Groningen. This is being achieved by using similar approaches to those employed to develop the
513 new r_d and MSF relationships for tectonic earthquakes (Lasley et al. 2016, 2017) to develop
514 Groningen-specific relationships using motions and soil profiles characteristic to Groningen.

515
516 The liquefaction hazard will be calculated using a Monte Carlo method wherein probability
517 distributions for activity rates, event locations and magnitudes, and resulting ground motions are
518 sampled such that the simulated future seismic hazard is consistent with historical seismic and
519 reservoir compaction datasets for events having magnitudes ranging from M 3.5 to 7.0. For each
520 event scenario, the Groningen-specific relationships will be used to compute the factor of safety
521 (FS_{liq}) against liquefaction as a function of depth for ~100 profiles across the liquefaction pilot
522 study area and corresponding Ishihara inspired Liquefaction Potential Index (LPI_{ish}) (Maurer et al.
523 2015a) hazard curves are being computed for each profile. The hazard curves specify the return
524 periods of different severities of surficial liquefaction manifestations, with the severities
525 corresponding to a return period of 2475 years being of interest per the NPR 9998-2017. This is in
526 marked contrast to previous liquefaction hazard studies performed for Groningen that used a
527 pseudo-probabilistic approach, where the FS_{liq} or LPI is computed for an earthquake scenario (i.e.,
528 ground motions and magnitude) corresponding to a given return period.

529
530 The framework of the liquefaction hazard pilot study is in complete accord with the safety
531 philosophy of the NPR 9998-2017 and is particularly well suited to the specific nature of the time-
532 dependent induced seismicity being considered. The results of the study will form the basis on
533 which decisions will be made regarding the need for implementing mitigation measures. The
534 liquefaction hazard study is benefiting significantly from the broader efforts to assess the regional
535 seismic hazard in Groningen, to include the development of a regional velocity model (Kruiver et
536 al. 2017a, b), site response model (Rodriguez-Marek et al. 2017), and ground-motion prediction
537 model (Bommer et al. 2017).

538
539

540 **Acknowledgments**

541
542 This research was partially funded by National Science Foundation (NSF) grants CMMI-1030564
543 and CMMI-1435494 and Nederlandse Aardolie Maatschappij B.V. (NAM). This support is
544 gratefully acknowledged. This study has also significantly benefited from enlightening discussions
545 with colleagues at Shell, Deltares, Arup, Fugro, Beca, and on the NEN liquefaction task force.
546 However, any opinions, findings, and conclusions or recommendations expressed in this material
547 are those of the authors and do not necessarily reflect the views of the NSF or NAM.

548

549 **References**

550

551 Bird JF, Bommer JJ (2004) Earthquake losses due to ground failure. *Engineering Geology*
552 75(2):147-179.

553

554 Bommer JJ, van Elk J (2017) Comment on ‘The maximum possible and the maximum expected
555 earthquake magnitude for production-induced earthquakes at the gas field in Groningen, the
556 Netherlands’ by Gert Zöller and Matthias Holschneider. *Bulletin of the Seismological Society of*
557 *America* 107(3):1564-1567.

558

559 Bommer JJ, Dost B, Edwards B, Stafford PJ, van Elk J, Doornhof D, Ntinalexis M (2016)
560 Developing an Application-Specific Ground-Motion Model for Induced Seismicity. *Bulletin of the*
561 *Seismological Society of America* 106(1):158–173.

562

563 Bommer JJ, Stafford PJ, Edwards B, Dost B, v. Dedem E, Rodriguez-Marek A, Kruiver P, van Elk
564 J, Doornhof D, Ntinalexis M (2017) Framework for a ground-motion model for induced seismic
565 hazard and risk analysis in the Groningen gas field, the Netherlands. *Earthquake Spectra*
566 33(2):481-498.

567

568 Boore DM (2005) SMSIM – Fortran programs for simulating ground motions from earthquakes:
569 Version 2.3 – A Revision of OFR 96-80, USGS Open-File Report 00-509, U.S. Geological Survey,
570 Reston VA.

571
572 Boulanger RW, Idriss IM (2014) CPT and SPT Based Liquefaction Triggering Procedures. Report
573 No. UCD/CGM-14/01, University of California at Davis, Davis, CA.
574
575 Bourne SJ, Oates SJ (2017) Extreme threshold failures within a heterogeneous elastic thin-sheet
576 account for the spatial-temporal development of induced seismicity within the Groningen gas field.
577 Journal of Geophysical Research: Solid Earth 122. DOI: 10.1002/2017JB014356.
578
579 Bourne SJ, Oates SJ, Bommer JJ, Dost B, van Elk J, Doornhof D (2015) A Monte Carlo method
580 for probabilistic seismic hazard assessment of induced seismicity due to conventional gas
581 production. Bulletin of the Seismological Society of America 105:1721–1738.
582
583 Bradley BA (2011) Correlation of significant duration with amplitude and cumulative intensity
584 measures and its use in ground motion selection. Journal of Earthquake Engineering 15:809–832.
585
586 Carter WL, Green RA, Bradley BA, Wotherspoon LM, Cubrinovski M (2016) Spatial Variation
587 of Magnitude Scaling Factors During the 2010 Darfield and 2011 Christchurch, New Zealand,
588 Earthquakes. Soil Dynamics and Earthquake Engineering 91:175-186.
589
590 Cetin KO (2000) Reliability-based assessment of seismic soil liquefaction initiation hazard. Ph.D.
591 Thesis, University of California at Berkeley, Berkeley, CA.
592
593 Darendeli MB, Stokoe II KH (2001) Development of a new family of normalized modulus
594 reduction and material damping curves. Geotechnical Engineering Report GD01-1, University of
595 Texas at Austin, Austin, TX.
596
597 Green RA, Bommer JJ (2018) What is the smallest earthquake magnitude that can trigger
598 liquefaction? Earthquake Spectra (*in review*).
599
600 Green RA, Terri GA (2005) Number of equivalent cycles concept for liquefaction evaluations -
601 revisited. Journal of Geotechnical and Geoenvironmental Engineering 131(4):477-488.

602
603 Green RA, Mitchell JK, Polito CP (2000). An energy-based excess pore pressure generation model
604 for cohesionless soils. Proceedings of The John Booker Memorial Symposium – Developments in
605 Theoretical Geomechanics (D.W. Smith and J.P. Carter, eds.), A.A. Balkema, Rotterdam, The
606 Neatherlands, 383-390.
607
608 Green RA, Lee J, White TM, Baker JW (2008) The significance of near-fault effects on
609 liquefaction. Proc. 14th World Conf. on Earthquake Engineering, Paper No. S26-019.
610
611 Green RA, Cubrinovski M, Cox B, Wood C, Wotherspoon L, Bradley B, Maurer B (2014) Select
612 liquefaction case histories from the 2010-2011 Canterbury earthquake sequence. Earthquake
613 Spectra 30:131-153.
614
615 Green RA, Maurer BW, van Ballegooy S (2018) The influence of the non-liquefied crust on the
616 severity of surficial liquefaction manifestations: Case history from the 2016 Valentine’s Day
617 earthquake in New Zealand. Proc. Geotechnical Earthquake Engineering and Soil Dynamics V
618 (GEESD V), Austin, TX, 10-13 June. (*in press*)
619
620 Hancock J, Bommer JJ (2005) The effective number of cycles of earthquake ground motion.
621 Earthquake Engineering and Structural Dynamics 34:637-664.
622
623 Idriss IM (1999) An update to the Seed-Idriss simplified procedure for evaluating liquefaction
624 potential. Proc., TRB Workshop on New Approaches to Liquefaction, Publication No. FHWA-
625 RD-99- 165, Federal Highway Administration.
626
627 Idriss IM, Boulanger RW (2008) Soil liquefaction during earthquakes. Monograph MNO-12,
628 Earthquake Engineering Research Institute, Oakland, CA, 261 pp.
629
630 Ishihara K (1985) Stability of natural deposits during earthquakes. Proc. 11th Intern. Conf. on Soil
631 Mechanics and Foundation Engineering, San Francisco, CA, USA, 1:321-376.
632

633 Iwasaki T, Tatsuoka F, Tokida K, Yasuda S (1978) A practical method for assessing soil
634 liquefaction potential based on case studies at various sites in Japan. Proc. 2nd Intern. Conf. on
635 Microzonation, Nov 26-Dec 1, San Francisco, CA, USA.

636

637 Kokusho T, Kaneko Y (2014) Dissipated & strain energies in undrained cyclic loading tests for
638 liquefaction potential evaluations. Proc. Tenth US National Conf. on Earthquake Engineering, July
639 21-25, 2014, Anchorage, Alaska, DOI: 10.4231/D3DR2P89D

640

641 Korff M, Wiersma A, Meijers P, Kloosterman F, de Lange G, van Elk J, Doornhof D (2017)
642 Liquefaction mapping for induced seismicity based on geological and geotechnical features. Proc.
643 3rd Intern. Conf. on Performance-Based Design in Earthquake Geotechnical Engineering (PBDIII),
644 Vancouver, Canada, 16-19 July, 2017.

645

646 Kruiver PP, Wiersma A, Kloosterman FH, de Lange G, Korff M, Stafleu J, Busscher F, Harting
647 R, Gunnink JL, Green RA, van Elk J, Doornhof D (2017a). Characterisation of the Groningen
648 subsurface for seismic hazard and risk modelling. Netherlands Journal of Geosciences 96(5):s215-
649 s233.

650

651 Kruiver PP, van Dedem E, Romijn R, de Lange G, Korff M, Stafleu J, Gunnink JL, Rodriguez-
652 Marek A, Bommer JJ, van Elk J, Doornhof D (2017b) An integrated shear-wave velocity model
653 for the Groningen gas field, The Netherlands, Bulletin of Earthquake Engineering. doi:
654 10.1007/s10518-017-0105-y.

655

656 Lasley S, Green RA, Rodriguez-Marek A (2016). A new stress reduction coefficient relationship
657 for liquefaction triggering analyses. Technical Note, Journal of Geotechnical and
658 Geoenvironmental Engineering 142(11):06016013-1.

659

660 Lasley S, Green RA, Rodriguez-Marek A (2017) Number of equivalent stress cycles for
661 liquefaction evaluations in active tectonic and stable continental regimes. Journal of Geotechnical
662 and Geoenvironmental Engineering 143(4):04016116-1.

663

664 Lunne T, Robertson PK, Powell JJM (1997) Cone Penetration Testing in Geotechnical Practice,
665 EF Spon/Blackie Academic, Routledge Publishers, London, United Kingdom, 312 pp.
666

667 Maurer BW, Green RA, Taylor, O-DS (2015a) Moving towards an improved index for assessing
668 liquefaction hazard: Lessons from historical data. *Soils and Foundations* 55(4):778-787.
669

670 Maurer BW, Green RA, Cubrinovski M, Bradley BA (2015b) Calibrating the Liquefaction
671 Severity Number (LSN) for competing liquefaction evaluation procedures: A case study in
672 Christchurch, New Zealand. Proc. 6th Intern. Conf. on Earthquake Geotechnical Engineering
673 (6ICEGE), Christchurch, New Zealand, 2-4 November.
674

675 Maurer BW, Green RA, Cubrinovski M, Bradley BA (2015c) Fines-Content Effects on
676 Liquefaction Hazard Evaluation for Infrastructure in Christchurch, New Zealand. *Soil Dynamics
677 and Earthquake Engineering* 76:58-68.
678

679 NPR 9998 (2017) Assessment of structural safety of buildings in case of erection, reconstruction
680 and disapproval – Basis rules for seismic actions: induced earthquakes. NEN, Delft, Netherlands.
681

682 National Research Council (NRC) (2016) State of the Art and Practice in the Assessment of
683 Earthquake-Induced Soil Liquefaction and Consequences. Committee on Earthquake Induced Soil
684 Liquefaction Assessment, National Research Council, The National Academies Press,
685 Washington, DC.
686

687 Polito CP, Green RA, Lee J (2008) Pore pressure generation models for sands and silty soils
688 subjected to cyclic loading. *Journal of Geotechnical and Geoenvironmental Engineering*
689 134(10):1490-1500.
690

691 Polito C, Green RA, Dillon E, Sohn C (2013) The effect of load shape on the relationship between
692 dissipated energy and residual excess pore pressure generation in cyclic triaxial tests. *Canadian
693 Geotechnical Journal* 50(9):1118-1128.
694

695 Rodriguez-Marek A, Kruiver PP, Meijers P, Bommer JJ, Dost B, van Elk J, Doornhof D (2017) A
696 regional site-response model for the Groningen gas field. Bulletin of the Seismological Society of
697 America 107(5):2067-2077.
698

699 Seed HB, Idriss IM (1971) Simplified procedure for evaluating soil liquefaction potential. Journal
700 of the Soil Mechanics and Foundations Division 97(SM9):1249–273.
701

702 Seed HB, Idriss IM, Makdisi F, Banerjee N (1975) Representation of irregular stress time histories
703 by equivalent uniform stress series in liquefaction analysis. Report Number EERC 75-29,
704 Earthquake Engineering Research Center, College of Engineering, University of California at
705 Berkeley, Berkeley, CA.
706

707 Stafford PJ, Zurek BD, Ntinalexis M, Bommer JJ (2018) Extensions to the Groningen ground-
708 motion model for seismic risk calculations: Component-to-component variability and spatial
709 correlation. This volume.
710

711 Ulmer KJ, Upadhyaya S, Green RA, Rodriguez-Marek A, Stafford PJ, Bommer JJ, van Elk J
712 (2018) A Critique of b-values Used for Computing Magnitude Scaling Factors. Proc. Geotechnical
713 Earthquake Engineering and Soil Dynamics V (GEESD V), Austin, TX, 10-13 June. (*in press*)
714

715 van Ballegooy S, Malan P, Lacrosse V, Jacka ME, Cubrinovski M, Bray JD, O'Rourke TD,
716 Crawford SA, Cowan H (2014) Assessment of liquefaction-induced land damage for residential
717 Christchurch. Earthquake Spectra 30(1):31-55.
718

719 van Elk J, Doornhof D, Bommer JJ, Bourne SJ, Oates SJ, Pinho R, Crowley H (2017) Hazard and
720 risk assessments for induced seismicity in Groningen. Netherlands Journal of Geoscience
721 96(5):s259-s269.
722

723 Whitman RV (1971) Resistance of soil to liquefaction and settlement. Soils and Foundations
724 11(4):59-68.
725

726 Yoshimi Y, Tokimatsu K, Kaneko O, Makihara Y (1984). Undrained cyclic shear strength of dense
727 Niigata sand. *Soils and Foundations*, 24(4):131-145.
728
729 Youd TL, Idriss IM, Andrus RD, Arango I, Castro G, Christian JT, Dobry R, Finn WDL, et al.
730 (2001) Liquefaction Resistance of Soils: Summary Report from the 1996 NCEER and 1998
731 NCEER/NSF Workshops on Evaluation of Liquefaction Resistance of Soils. *Journal of*
732 *Geotechnical and Geoenvironmental Engineering* 127(4):297-313.